Long-wavelength fluctuations and the glass transition in two dimensions and three dimensions

Skanda Vivek[a,1], Colm P. Kelleher[b,c], Paul M. Chaikin[b,c], and Eric R. Weeks[a]

[a]Department of Physics, Emory University, Atlanta, GA 30322; [b]Department of Physics, New York University, New York, NY 10003; and [c]Center for Soft Matter Research, New York University, New York, NY 10003

Edited by Andrea J. Liu, University of Pennsylvania, Philadelphia, PA, and approved October 19, 2016 (received for review May 9, 2016)

Phase transitions significantly differ between 2D and 3D systems, but the influence of dimensionality on the glass transition is unresolved. We use microscopy to study colloidal systems as they approach their glass transitions at high concentrations and find differences between two dimensions and three dimensions. We find that, in two dimensions, particles can undergo large displacements without changing their position relative to their neighbors, in contrast with three dimensions. This is related to Mermin–Wagner long-wavelength fluctuations that influence phase transitions in two dimensions. However, when measuring particle motion only relative to their neighbors, two dimensions and three dimensions have similar behavior as the glass transition is approached, showing that the long-wavelength fluctuations do not cause a fundamental distinction between 2D and 3D glass transitions.

colloidal glass transition | dimensionality | long-wavelength fluctuations | phase transition | two-dimensional physics

If a liquid can be cooled rapidly to avoid crystallization, it can form into a glass: an amorphous solid. The underlying cause of the glass transition is far from clear, although there are a variety of theories (1–3). One recent method of understanding the glass transition has been to simulate the glass transition in a variety of dimensions (including four dimensions or higher) (4–8). Indeed, the glass transition is often thought to be similar in two and three dimensions (9, 10), and in simple simulation cases such as hard particles, one might expect that dimensionality plays no role. As a counterargument, 2D and 3D fluid mechanics are qualitatively quite different (11). Likewise, melting is also known to be qualitatively different in two and three dimensions (12–15).

Recent simulations give evidence that the glass transition is also quite different in two and three dimensions (4, 5). In particular, Flenner and Szamel (4) simulated several different glass-forming systems in two and three dimensions and found that the dynamics of these systems were fundamentally different in two and three dimensions. They examined translational particle motion (motion relative to a particle's initial position) and bond-orientational motion (topological changes of neighboring particles). They found that, in two dimensions, these two types of motion became decoupled near the glass transition. In these cases, particles could move appreciable distances but did so with their neighbors, so that their local structure changed slowly. In three dimensions, this was not the case; translational and bond-orientational motions were coupled. They additionally observed that the transient localization of particles well known in three dimensions was absent in the 2D data. To quote Flenner and Szamel, "these results strongly suggest that the glass transition in two dimensions is different from in three dimensions."

In this work, we use colloidal experiments to test dimension-dependent dynamics approaching the glass transition. Colloidal samples at high concentration have been established as model glass formers (10, 16–19). We perform microscopy experiments with two 2D bidisperse systems, one with quasihard interactions, and the other with long-range dipolar interactions. Three-dimensional data are obtained from previous experiments by Narumi et al. (20), which studied a bidisperse mixture of hard particles. Our results are in qualitative agreement with the simulations of Flenner and Szamel.

We believe our observations are due to the Peierls instability (21, 22), also called Mermin–Wagner fluctuations (23, 24). As Peierls originally argued, there exist long-range thermal fluctuations in positional ordering in 1D and 2D solids. Illing et al. (25) and Klix et al. (26) recently noted that these arguments should apply to disordered systems as well. One can measure particle motion relative to the neighbors of that particle to remove the influence of these long-wavelength fluctuations (27). Using this method, we observe that the translational and structural relaxations are similar between two dimensions and three dimensions, demonstrating that the underlying glass transitions are unaffected by the Mermin–Wagner fluctuations.

Results

We analyze three different types of colloidal samples, all using bidisperse mixtures to avoid crystallization. The first sample type is a quasi-2D sample with hard particles (short range, purely repulsive interactions), which we term "2DH." The 2DH sample is made by allowing silica particles to sediment to a monolayer on a coverslip (28). Our 2DH system is analogous to a 2D system of hard disks of the sort studied with simulations (9, 29). The control parameter is the area fraction ϕ, with glassy samples found for $\phi \geq 0.79$. The second sample type is also quasi-2D but with softer particles, which we term "2DS." The 2DS system is composed of bidisperse poly-methyl-methacrylate (PMMA) particles dispersed in oil, at an oil–aqueous interface (30). The interactions in this system are dipolar in the far-field limit, and the control parameter is the dimensionless interaction parameter Γ_{2DS}, related to the area fraction. Γ_{2DS} is defined in *Materials and Methods*, with glassy behavior found for $\Gamma \geq 530$. For the third sample type, "3D," we use previously published 3D data on a bidisperse sample of hard-sphere–like colloids (20).

Significance

For phase transitions and fluid dynamics, there are significant qualitative differences between two dimensions and three dimensions. However, it has been long assumed that the glass transition is similar in two and three dimensions. Here, we present experimental data on 2D and 3D colloidal systems near their glass transitions. We demonstrate that the differences between two dimensions and three dimensions are due to long-wavelength fluctuations, precisely those that distinguish 2D and 3D phase transitions. We show that the influence of these fluctuations can be disentangled from the underlying dynamics, and that 2D and 3D glass transitions are otherwise similar.

Author contributions: S.V., C.P.K., P.M.C., and E.R.W. designed research; S.V. and C.P.K. performed research; S.V., C.P.K., P.M.C., and E.R.W. contributed new reagents/analytic tools; S.V. analyzed data; and S.V. and E.R.W. wrote the paper.

The authors declare no conflict of interest.

This article is a PNAS Direct Submission.

[1]To whom correspondence should be addressed. Email: skanda.vivek@gmail.com.

For these data, the control parameter is the volume fraction ϕ with glasses found for $\phi \geq 0.58$ (20). Details of the sample preparation and data acquisition for these three sample types are in *Materials and Methods*. For each sample type, the glass transition is defined as the parameter (Γ or ϕ) above which the sample mean-square displacement (MSD) does not equilibrate in experimental timescales, ~ 10 h for the 2D samples and ~ 3 h for the 3D samples.

Flenner and Szamel found that, in two dimensions, particles move large distances without significantly changing local structure (4). They noted that timescales for translational motion and timescales for changes in local structure were coupled in three dimensions, but not in two dimensions. The standard way to define these timescales is through autocorrelation functions. Following ref. 4, we compute the self-intermediate scattering function $F_S(k, \Delta t)$ to characterize translational motion, and a bond-orientational correlation function $C(\Delta t)$ to characterize changes in local structural configuration (see *Materials and Methods* for details). These are plotted in Fig. 1 *A–C* and 1 *D–F*, respectively. At short timescales, particles have barely moved, and so both of these correlation functions are close to 1. At longer timescales, these functions decay, taking longer timescales to do so at larger concentrations. The traditional relaxation timescale τ_α is defined from $F_S(\tau_\alpha) = 1/e = 0.37$. For the bond-orientational correlation functions, we quantify local arrangements of particles through ψ_6 in two dimensions and Q_6 in three dimensions, both of which are sensitive to hexagonal order (31). Decay of the autocorrelation functions for these quantities (Fig. 1 *D–F*) reflects how particles move relative to one another, thus changing their local structure, whereas decay of F_S reflects motion relative to each particle's initial position.

Specifically, Flenner and Szamel found that $F_S(\Delta t)$ and $C(\Delta t)$ had qualitatively different decay forms in two dimensions, but were similar in three dimensions (4). In particular, $F_S(\Delta t)$ decayed significantly faster than $C(\Delta t)$ for 2D simulations. This means that, in two dimensions, particles could move significant distances (of order their interparticle spacing) but did so in parallel with their neighbors, so that their positions were changed but not their local structure.

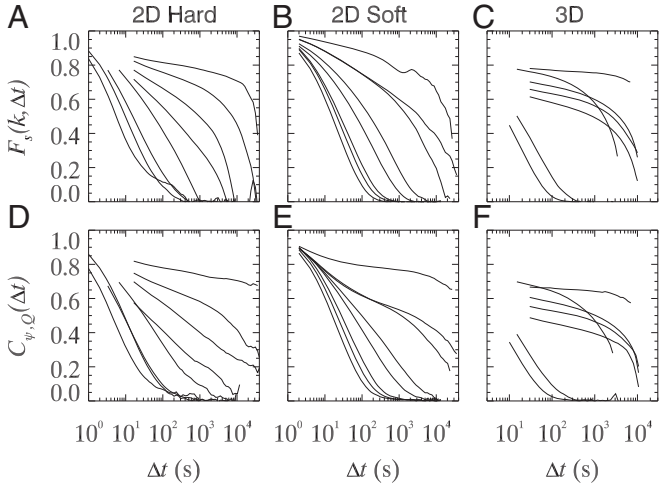

Fig. 1. Structural relaxation in two and three dimensions. (*A–C*) Self-intermediate scattering functions characterizing translational motion, using the wave vector *k* corresponding to the peak of the structure factor (*Materials and Methods*). (*D–F*) Bond-orientational correlation functions. The columns correspond to 2DH, 2DS, and 3D experiments. The parameters for the experiments are as follows: $\phi_{2DH} = 0.55$, 0.65, 0.70, 0.74, 0.75, 0.76, 0.78, and 0.78; 2DS ($\Gamma_{2DS} = 60$, 100, 100, 140, 180, 310, 300, and 460); 3D $\phi_{3D} = 0.40$, 0.42, 0.52, 0.53, 0.54, 0.54, and 0.58. These parameters increase from *Left* to *Right* in each panel; or equivalently, from *Bottom* to *Top*.

To compare translational and bond orientational correlation functions of our data, we replot some of the data in Fig. 2 *A–C*. The translational correlation functions for different parameters are solid curves with different colors. The bond-orientational correlation functions are dashed curves, with same color as corresponding translational correlation functions.

The 2D data of Fig. 2 *A–B* exhibit decoupling, whereas the 3D data of *C* are coupled. For the latter case, coupling means that the two functions decrease together, and their relative positions do not change dramatically as the glass transition is approached. Even for the most concentrated case, for which we do not observe a final decay of either function, it still appears that the two correlation functions are related and starting an initial decay around the same timescale. In contrast, for both 2D cases (Fig. 2 *A*, *B*), F_S and C_ψ change in relation to one another as the glass transition is approached. For 2DH (*A*), at the most liquid-like concentration (black curves), *C* decays faster than F_S (dashed curve compared with the solid curve). As the glass transition is approached, initially *C* decays faster, but then the decay of F_S overtakes *C*. A similar trend is seen for 2DS (*B*). For both 2DH and 2DS, the decoupling is most strongly seen for the most concentrated samples (green curves), for which $F_S(\Delta t)$ decays on experimental timescales but where $C_\psi(\Delta t)$ decays little on the same timescales.

The slower decay of bond-orientational correlations relative to translational correlations for our 2D data is in good qualitative agreement with Flenner and Szamel's observations (4). Upon approaching the glass transition in two dimensions, particles are constrained to move with their neighbors such that *C* decays less than might be expected on timescales where F_S has decayed significantly. In three dimensions, however, on approaching the glass transition, particles move in a less correlated fashion. To quantify the correlated motion of neighboring particles, we compute a two-particle correlation function (9, 32). This function correlates the vector displacements of pairs of nearest neighbor particles (*Materials and Methods*). Fig. 3 shows these correlations: 1 corresponds to complete correlation, and 0 is completely uncorrelated. For both 2D samples (solid symbols), the correlations increase for larger τ_α, as indicated by the fit lines. This increased correlation reflects particles moving in parallel directions with their nearest neighbors. For the 3D data (open squares in Fig. 3), the correlations are small and do not grow as the glass transition is approached. Particle motion uncorrelated with neighboring particles decorrelates both positional information and bond-orientational structure.

To qualitatively visualize the differences between dynamics in two dimensions and three dimensions, the top row of Fig. 4 shows displacement vectors for particles in the three samples near their glass transitions. For both 2DH and 2DS samples, there are clusters of particles moving in similar directions as seen by adjacent displacement arrows pointing in a similar direction. This clustering is less pronounced in three dimensions, consistent with the small correlations between nearest neighbor motions in three dimensions (Fig. 3).

As suggested in the Introduction, it is plausible that some of the significant translational motion in the 2D samples is due to Mermin–Wagner fluctuations, which act at long wavelengths (25, 33). To disentangle the potential influences of long-wavelength fluctuations from relative motions, we subtract collective motions by measuring "cage relative" particle motions (27). The key idea is to measure displacements relative to the average displacements of each particle's nearest neighbors, that is, relative to the cage of neighbors surrounding each particle. Previous work has shown that using cage-relative coordinates reveals the dynamical signatures of phase transitions for systems of monodisperse colloids (14). We compute these

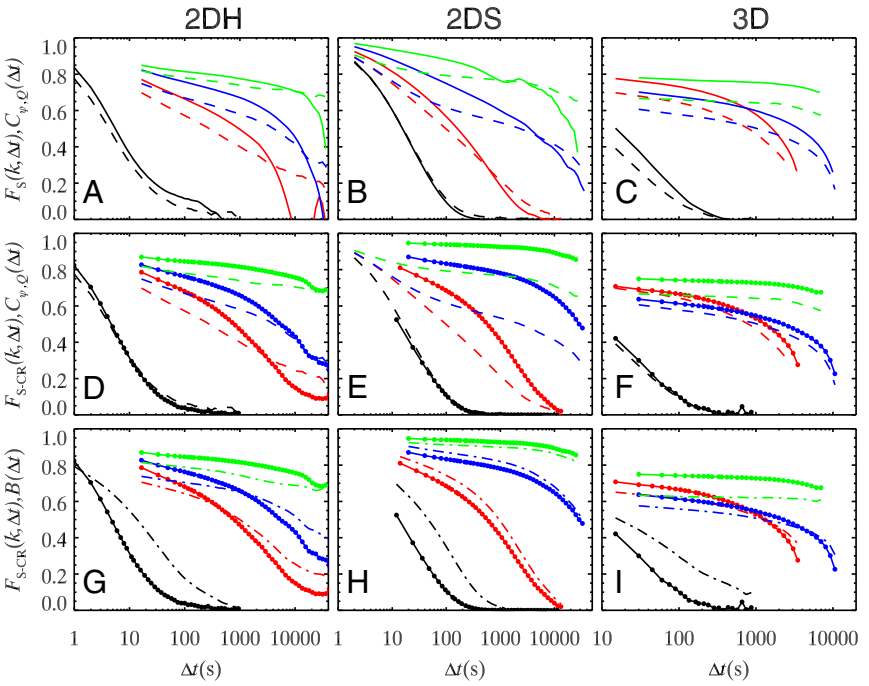

Fig. 2. Translational, bond-orientational, and bond-break correlation functions. (*A–C*) The solid curves are $F_S(\Delta t)$ (translational correlations) and the dashed curves are $C(\Delta t)$ (bond-orientational correlations) for the 2DH, 2DS, and 3D samples as labeled. The colors indicate different control parameters. For 2DH, the colors black, red, blue, and green denote $\phi_{2DH} = 0.55$, 0.75, 0.78, and 0.78, respectively. For 2DS, the colors black, red, blue, and green denote $\Gamma_{2DS} = 60$, 180, 310, and 460, respectively. For 3D, the colors black, red, blue, and green denote $\phi_{3D} = 0.42$, 0.52, 0.54, and 0.58, respectively. (*D–F*) The solid curves with circles are $F_{S-CR}(\Delta t)$ (cage-relative translational correlations). The dashed curves are $C(\Delta t)$, which are identical to those shown in (*A–C*). (*G–I*) The solid curves with circles are $F_{S-CR}(\Delta t)$ (cage-relative translational correlations) and the dot-dashed curves are $B(\Delta t)$ (bond-break correlations) for the 2DH, 2DS, and 3D samples.

cage-relative displacements and then calculate the self-intermediate scattering function F_{S-CR} using these new displacements. These are plotted as solid lines with circles in Fig. 2 *D–F*, with the dashed lines being the bond-orientational data [which are unchanged as $C(\Delta t)$ is always calculated relative to neighbors]. In both 2DH and 2DS, $F_{S-CR}(\Delta t) > F_S(\Delta t)$ (the solid lines in Fig. 2 *D*, *E* are higher than the corresponding solid lines in Fig. 2 *A*, *B*). This is expected given the arguments above, that particles move with their neighbors, hence subtracting nearest-neighbor motions results in reduction of particle mobility. For the 3D data (Fig. 2*F*), the $F_{S-CR}(\Delta t)$ curves still show coupling to $C_Q(\Delta t)$ similar to the original data shown in Fig. 2*C*.

To provide a complementary view, we consider another measure of structural changes, the cage correlation function (or bond-breaking function) $B(\Delta t)$. $B(\Delta t)$ is the fraction of particles that have the same neighbors at times t and $t+\Delta t$, averaged over t (34, 35).

These functions are plotted in Fig. 2 *G–I* as dash-dotted lines and are compared with F_{S-CR}. The black curves are the lowest concentrations, which all have $B(\Delta t) > F_{S-CR}(\Delta t)$. This is because, at lower concentrations, particles can translate a significant amount without losing neighbors. However, at larger concentrations, $B(\Delta t) \sim F_{S-CR}(k, \Delta t)$ in all three types of samples. For all three experiments, the two correlation functions look fairly similar at the three highest concentrations shown in Fig. 2 *G–I*. In particular, the differences between the 2D and 3D data are much reduced compared with the original analysis shown in *A–C*.

In fact, our strongest qualitative evidence for coupling comes from comparison of the green curves in Fig. 2, which are the samples closest to the glass transition. In each case, the correlation functions do not fully decay within our experimental observation time. Nonetheless, it is apparent for the 2D data that the normal self-intermediate scattering function is beginning a final decay at a timescale for which the bond-orientational function has not

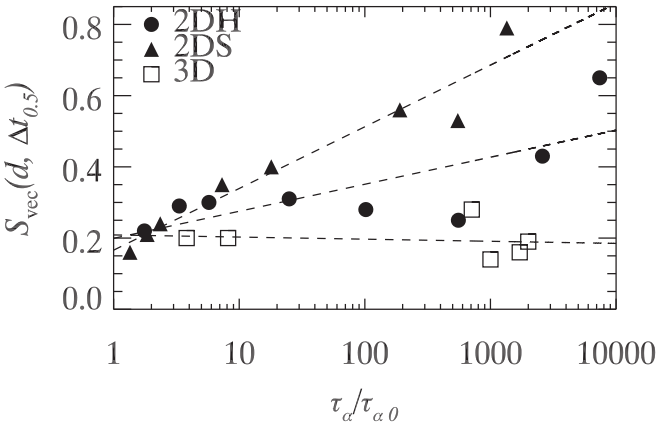

Fig. 3. Vector displacement correlations. The data are for 2DH (filled circles), 2DS (filled triangles), and 3D (open squares). The displacements are calculated using a timescale Δt such that $F_S(\Delta t) = 0.5$. These are measured for all pairs of particles separated by the nearest-neighbor spacing *d*. *d* is determined from the large–large peak position in the pair correlation function $g(r)$ at the highest concentrations, and has values $d = 3.38$, 6.5, and 3.10 μm for 2DH, 2DS, and 3D, respectively. [The location of the $g(r)$ peak depends slightly on ϕ for 2DH and 3D experiments, and more strongly on Γ for the 2DS experiments; for consistency, we keep *d* fixed to these specific values.] The lines are least-squares fits to the data. The data are plotted as a function of $\tau_\alpha/\tau_{\alpha 0}$ where $\tau_{\alpha 0}$ is the relaxation timescale for the large particles in a dilute sample. The 2DH (closed circles), 2DS (closed triangles), and 3D (open squares) samples have $\tau_{\alpha 0} = 5.4$, 20, and 3.8 s, respectively.

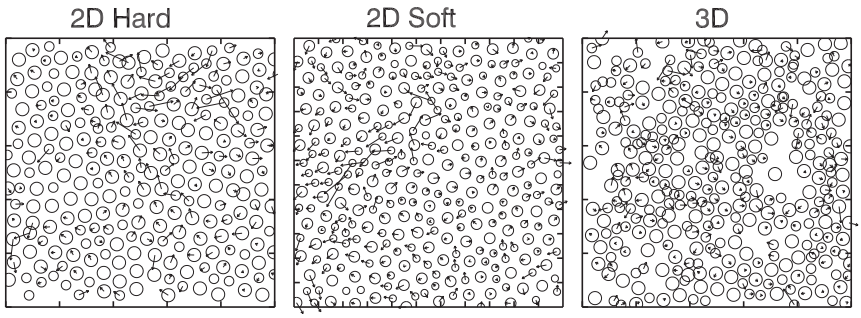

Fig. 4. Particle displacements. These images show displacement vectors of particles using a time interval Δt chosen such that $F_s(\Delta t) = 0.5$. For the 3D image, we use an *xy* cut at fixed *z*. All scale ticks are at 10-μm intervals, and all displacement vectors are multiplied by 2 for easier visualization. The circles denote particle positions and sizes. Samples are $\phi_{2DH} = 0.78$, $\Gamma_{2DS} = 300$, and $\phi_{3D} = 0.54$, from left to right, with corresponding $\Delta t = 4{,}290$, 1,720, and 3,540 s. τ_α for these samples are 14,000, 3,800, and 7,600 s, respectively. Circles with no arrows are those with displacements less than 10% of symbol size.

yet begun to decay (Fig. 2 *A*, *B*). This is not the case for the 3D data (*C*). In contrast, all three datasets exhibit similar behavior at the largest timescales when comparing the cage-relative $F_{S-CR}(k, \Delta t)$ and $B(\Delta t)$ (*G*–*I*).

We turn now to the question of transient localization, which Flenner and Szamel found to be present in three dimensions but not two dimensions. The trajectories of 3D particles showed localized motions separated by abrupt jumps, whereas trajectories of 2D particles did not have these two distinct types of motion (4). In their data, this caused a plateau in the 3D MSD, which was not seen in the 2D MSD. The plateau is due to particles being transiently trapped in cages formed by their neighbors, with the plateau height set by the cage size (35).

Motivated by the considerations above, we investigate the cage-relative mean square displacements (CR-MSDs) (27). In analogy with the cage-relative scattering function, we use the cage-relative displacement $\Delta\vec{r}_{CR}$ to define the CR-MSD. Fig. 5 shows the original MSD data (thin lines) and CR-MSD (lines with circles). For all experiments, as the concentration increases, the MSD drops, reflecting the slowing dynamics on approaching the glass transition. In some cases, the CR-MSD is larger than the MSD (for example, all of the curves in Fig. 5*C*). In these situations, the motion of each particle is less correlated with the motion of its neighbors, so the cage-relative analysis effectively adds a random vector to each particle's displacement, thus increasing the MSD on average. However, for the 2D samples as they approach the glass transition, the opposite occurs. Especially for the green curves in Fig. 5 *A*, *B*, the data closest to the glass transition, it is clear that the cage-relative analysis dramatically decreases the CR-MSD data relative to the original MSD. Although we show data close to the glass transition, none of our data are from glasses. There have been a number of experiments on other 2D colloidal systems such as soft particles (36) and attractive particles (37), which observed a slowly rising MSD for glasses. Our results suggest that the MSD rise seen in these prior experiments may also disappear with cage-relative analysis, strengthening the argument that these prior experiments studied truly glassy samples.

To quantify transient localization, we measure the instantaneous logarithmic MSD slope γ from $\langle \Delta r^2 \rangle \sim \Delta t^{\gamma(\Delta t)}$. $\gamma = 1$ corresponds to normal diffusion. We quantify the amount of localization by the minimum value of this slope, γ_{min}; this is the logarithmic slope at the inflection point of the MSD or CR-MSD. Fig. 6*A* shows the CR data for the 2D samples (filled symbols) and 3D (open squares) as a function of τ_α. Although the 3D data reach lower values, the overall trend is similar between two dimensions and three dimensions: the closer to the glass transition, the more pronounced transient localization is. Note that, in the work of Flenner and Szamel, they tested both Newtonian dynamics and Brownian dynamics; the latter is more appropriate for colloids. With Brownian dynamics in two dimensions, they found slightly more pronounced MSD plateaus. It is possible that the presence of Brownian dynamics in our

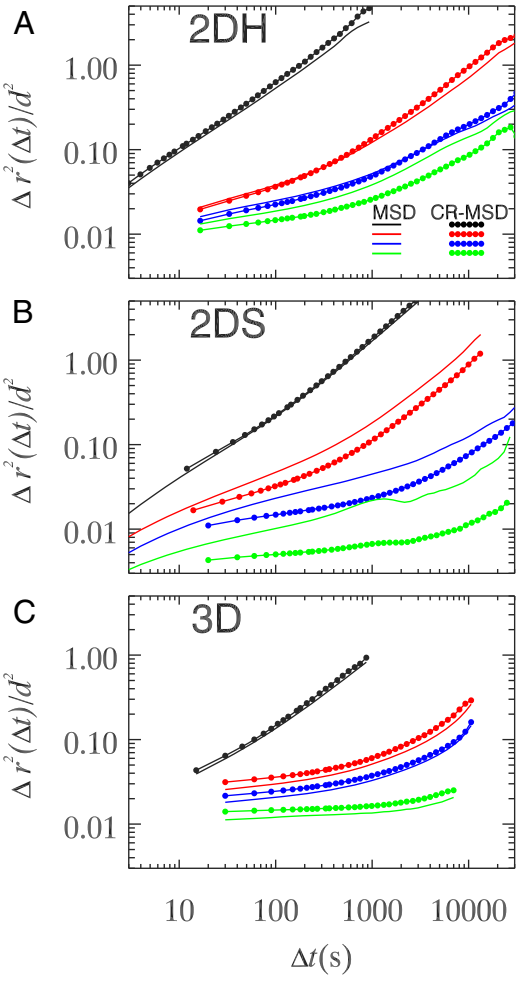

Fig. 5. MSDs and cage-relative MSDs. The data (*A*–*C*) are for the experiments as indicated. The solid curves are MSDs $\langle \Delta r^2 \rangle$ calculated for all particles, normalized by *d* as described in the legend to Fig. 3. The solid curves with circles are cage-relative MSDs. The colors indicate different control parameters, as given in Fig. 2. For the 3D samples, the *z* direction is neglected due to noise and also to facilitate the comparison with the 2D experiments.

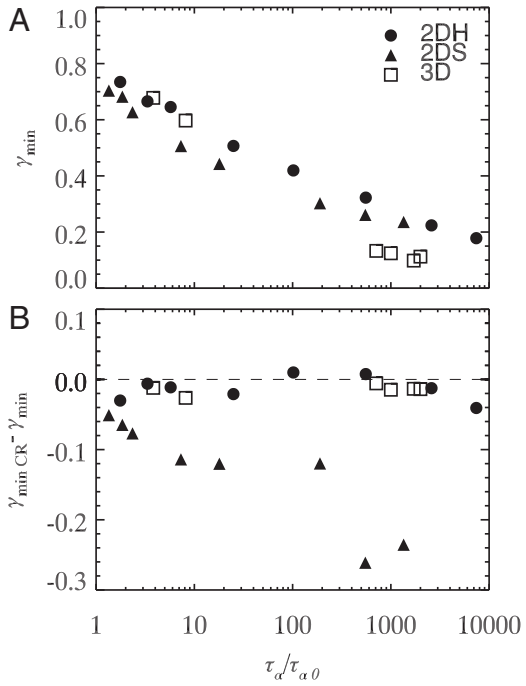

Fig. 6. Transient localization parameter. (*A*) $\gamma_{min,CR}$ is the minimum logarithmic slope of the cage-relative MSDs. (*B*) Difference $\gamma_{min,CR} - \gamma_{min}$ between the original MSD data and the cage-relative version. Negative values indicate the enhancement of measured transient localization using the cage-relative analysis.

experiments also contributes to our observed similarities in transient localization between two dimensions and three dimensions.

Fig. 6*B* shows the slight enhancement of transient localization caused by the cage-relative analysis. We plot the change in γ_{min} upon using the cage-relative analysis, and it is generally negative. The largest changes are seen in the 2DS data (solid triangles), which is sensible as these are the data with the strongest correlations with their neighbors.

Discussion

Our experiments show apparent differences in dynamics approaching the 2D and 3D colloidal glass transition, in agreement with the simulation results of Flenner and Szamel (4).

In two dimensions, we observe that particles move in parallel with their neighbors, such that their local structure changes less than if the motions were uncorrelated. Although it is clear from prior work that in three dimensions particle motions have some correlation with their neighbors (32), in our data the correlations are more significant for the 2D samples. These are likely related to Mermin–Wagner fluctuations/the Peierls instability in two dimensions (21–26).

Our 2D samples are, of course, quasi-2D. Both are influenced by nearby large 3D regions of fluid. The 2DH sample also has hydrodynamic interactions between particles and the nearby bottom of the sample chamber. We find that 2DS samples are more affected by long-wavelength fluctuations than 2DH, which could be due to the difference in interactions (24, 38). It is certainly plausible that softer interactions allow for more fluctuations in the nearest-neighbor distance, whereas for dense samples with hard interactions, fluctuations are by necessity smaller (as particles cannot move too close together before they repel) (25). Recent simulation work has shown differences in correlation lengths for disks with soft and hard interaction potentials during 2D melting (39). Nonetheless, the agreement between the two 2D datasets is striking, especially given the different particle interaction potentials; namely, as distinct from the 3D samples, both 2D samples show large Mermin–Wagner fluctuations.

Another important experimental factor is the system size: approximately $10^5 - 10^6$ for both 2D systems and 10^9 for the 3D system. It is likely that for even larger 2D systems, the Mermin–Wagner fluctuations would be more pronounced (4, 33, 40).

Klix et al. (26) recently argued that Mermin–Wagner fluctuations should be present in glassy systems. Probably the most interesting aspect of our study is the suggestion that indeed 2D Mermin–Wagner fluctuations are present in our amorphous samples. Mermin–Wagner fluctuations conventionally result from elasticity associated with the development of an order parameter. The origin of elasticity in glassy systems is less well understood. Although we have not proven that our observed long-wavelength fluctuations are indeed Mermin–Wagner fluctuations, one could vary the system size in future investigations to examine how the difference between conventional and cage-relative measurements depends on system size. In conclusion, with our efforts and other recent work, there is a compelling collection of evidence that 2D and 3D glass transitions are fundamentally the same: there is strong qualitative agreement between our observations studying three colloidal systems, the colloidal experiments and simulations of Illing et al. (25), and the soft-particle simulations of Shiba et al. (33). The similarities between the conclusions, despite the differences in methods and dynamics, suggest the results are independent of the details. All of these observations show that the 2D glass transition is similar to the 3D glass transition, but with the added influence of Mermin–Wagner fluctuations in two dimensions.

Materials and Methods

For 2DH experiments, we confine bidisperse nonfunctionalized silica particles (diameters, $\sigma_S = 2.53$ and $\sigma_L = 3.38$ μm; Bangs Laboratories; SS05N) to a monolayer by gravity. Before taking data, the sample is quenched by shaking and letting particles sediment on the coverslip. The coverslip is made hydrophobic by treatment with Alfa Aesar Glassclad 18 to prevent particle adhesion. All particles are observed to move during the experiment; none adhere to the glass. We do not add salt. The sedimentation lengths for both small ($l_g/\sigma_S = 0.019$) and large particles ($l_g/\sigma_L = 0.006$) are small enough to ensure fast sedimentation and formation of a quasi-2D monolayer; that is, thermal energy is not enough to overcome the gravitational potential energy of the particles (10). We verify that, in all experiments, only one layer of particles is present (ensured by keeping the overall particle concentration below the level that requires a second layer to form). We use bright-field microscopy and a CCD camera to record movies of particles diffusing. This system is analogous to 2D hard disks. The only caveat is that the centers of the large and small particles are not at the same height, so adjacent large and small particles do not contact each other at their midplane (41).

For 2DS, the experimental system is composed of bidisperse PMMA colloids of diameters 1.1 and 2.6 μm. The particles are at the interface between oil and a glycerol/water mixture. The aqueous phase consists of 10 mM NaCl, 70 wt% glycerol solution, whereas the oil phase consists of a 50–30–20 (vol/vol) mixture of cyclohexyl bromide, hexane, and dodecane. Interactions between particles are dipolar in the far-field limit. A dimensionless interaction parameter (18) is used to characterize the system:

$$\Gamma_{2DS} = \frac{(\pi n)^{3/2}}{8\pi\epsilon k_B T}(\xi p_B + (1-\xi)p_A)^2 \qquad [1]$$

where $\epsilon = 4.2\epsilon_0$. The electric dipole moments are p_A and $p_B = 2{,}300$ and 590 $e \cdot \mu$m, respectively. $\xi \approx 0.57 - 0.83$ is the number fraction of small particles, and n is the areal density, measured from a Voronoi tessellation.

The 3D sample data were obtained from a previous experiment by Narumi et al. (20). In the 3D experiments, PMMA colloids were stabilized sterically by a thin layer of poly-12-hydroxy-stearic acid. A binary mixture with diameters $\sigma_L = 3.10$ μM and $\sigma_S = 2.36$ μm were used. The number ratio of small particles to large particles was 1.56.

The imaging regions encompass roughly 400, 1,500, and 2,000 particles for 2DH, 2DS, and 3D samples, respectively, at their highest concentrations. The total system sizes are much larger, approximately $10^5 - 10^6$ for both 2D systems and 10^9 for the 3D system. We postprocessed 2DH and 2DS movies using particle-tracking algorithms (42) to extract particle positions from individual frames. The 3D data were previously tracked using the same

algorithm. Our uncertainty in particle position is 0.1 μm for the 2DH experiment, 0.5 μm for the 2DS experiment, and 0.2 μm (x, y) and 0.3 μm (z) for the 3D experiment (20).

The α relaxation timescales are computed from self-intermediate scattering functions: $F_S(k, \Delta t) = \langle \exp(i\vec{k} \cdot \Delta\vec{r}) \rangle_t$, where $\Delta\vec{r} = \vec{r}(t + \Delta t) - \vec{r}(t)$. The wave vector k corresponds to the peak of the structure factor $S(\vec{k}) = \langle N^{-1} | \sum_{i=1}^{N} \exp(i\vec{k} \cdot \vec{r}_i(t))|^2 \rangle$, where $\vec{r}_i(t)$ denotes particle positions at time t and the average is over all times. Corresponding to 2DH, 2DS, and 3D, $k = 2.2$, 1.0, and 2.6 μm^{-1}, obtained using the average k across all samples of a particular type.

Several other functions we compute require identifying nearest neighbors, which we do using the Voronoi tessellation (17).

We define cage-relative translational correlation function as follows: $F_{S-CR}(k, \Delta t) = \langle \exp(i\vec{k} \cdot \Delta\vec{r}_{CR}) \rangle_t$, where $\Delta\vec{r}_{CR} = \vec{r}(t+\Delta t) - \vec{r}(t) - \frac{1}{N}\sum_j [\vec{r}_j(t + \Delta t) - \vec{r}_j(t)]$, j denotes nearest neighbors of the particle at initial time t, and the sum is over all neighbors. The cage-relative MSD is defined using the same displacements $\Delta\vec{r}_{CR}$.

To measure bond-orientational correlations in two dimensions (4), we define $\Psi_6^n(t) = \sum_m (N_b^n)_m^{-1} e^{i6\theta_m}$, where m are the nearest neighbors of particle n and θ_m is the angle made by particle m with defined axis. From this, the bond-orientational correlation function can be found as $C_\Psi(\Delta t) = \langle \sum_n [\Psi_6^n(t)]^* \Psi_6^n(t + \Delta t) \rangle_t / \langle \sum_n |\Psi_6^n(t)|^2 \rangle_t$.

In three dimensions, we define $Q_{lm}^i(t) = (N_b^i)^{-1} \sum_j q_{lm}[\theta_{ij}(t), \phi_{ij}(t)]$, where $q_{lm}(\theta, \phi)$ are spherical harmonics (4, 31) and the sum is over neighbors of particle i. Next, we define the correlation function $Q_l(t_1, t_2) = 4\pi/(2l+1) \sum_i \sum_{m=-l}^{l} Q_{lm}^i(t_2)[Q_{lm}^i(t_1)]^*$. We calculate $C_Q(\Delta t) = \langle Q_6(t, t + \Delta t) \rangle_t / \langle Q_6(t, t) \rangle_t$ corresponding to $l = 6$, given that $l = 6$ is sensitive to hexagonal order known to be present even in disordered samples.

The two-particle vector correlations are determined from a spatial-temporal correlation function defined as $S_{\text{vec}}(R, \Delta t) = \langle \Delta\vec{r}_i \Delta\vec{r}_j \rangle_{\text{pair}} / \langle (\Delta\vec{r}^2) \rangle$ (9, 32). The average is over all particles with initial separation $R \approx d$, and over the initial time t. For the initial separation R, we use $R = 3.38 \pm 0.2$, $R = 6.5 \pm 0.4$, and $R = 3.1 \pm 0.2$ μm for the 2DH, 2DS, and 3D data. To determine the displacements $\Delta\vec{r}$, we use the timescale Δt such that $F_S(\Delta t) = 0.5$. This is chosen to be a shorter timescale than τ_α, as particle displacements are typically maximally spatially heterogeneous at a shorter timescale (17, 35).

ACKNOWLEDGMENTS. We thank E. Flenner, G. Szamel, R. Guerra, P. Keim, H. Shiba, and V. Trappe for useful discussions. This work was supported by National Science Foundation Grant CMMI-1250235 (to S.V. and E.R.W.), National Science Foundation Grant DMR-1105417 (to C.P.K. and P.M.C.), National Aeronautics and Space Administration Grant NNX 13AR67G, and National Science Foundation Materials Research Science and Engineering Center Program Grant DMR-1420073.

1. Biroli G, Garrahan JP (2013) Perspective: The glass transition. *J Chem Phys* 138:12A301.
2. Ediger MD, Harrowell P (2012) Perspective: Supercooled liquids and glasses. *J Chem Phys* 137:080901.
3. Cavagna A (2009) Supercooled liquids for pedestrians. *Phys Rep* 476:51–124.
4. Flenner E, Szamel G (2015) Fundamental differences between glassy dynamics in two and three dimensions. *Nat Commun* 6:7392.
5. Sengupta S, Karmakar S, Dasgupta C, Sastry S (2012) Adam-Gibbs relation for glass-forming liquids in two, three, and four dimensions. *Phys Rev Lett* 109:095705.
6. van Meel JA, Frenkel D, Charbonneau P (2009) Geometrical frustration: A study of four-dimensional hard spheres. *Phys Rev E Stat Nonlin Soft Matter Phys* 79:030201.
7. Charbonneau P, Ikeda A, van Meel JA, Miyazaki K (2010) Numerical and theoretical study of a monodisperse hard-sphere glass former. *Phys Rev E Stat Nonlin Soft Matter Phys* 81:040501.
8. Charbonneau P, Ikeda A, Parisi G, Zamponi F (2011) Glass transition and random close packing above three dimensions. *Phys Rev Lett* 107:185702.
9. Doliwa B, Heuer A (2000) Cooperativity and spatial correlations near the glass transition: Computer simulation results for hard spheres and disks. *Phys Rev E Stat Phys Plasmas Fluids Relat Interdiscip Topics* 61:6898–6908.
10. Hunter GL, Weeks ER (2012) The physics of the colloidal glass transition. *Rep Prog Phys* 75:066501.
11. Tritton DJ (1988) Physical Fluid Dynamics. Oxford Science Publications (Oxford Univ Press, Oxford, UK), 2nd Ed.
12. Bernard EP, Krauth W (2011) Two-step melting in two dimensions: First-order liquid-hexatic transition. *Phys Rev Lett* 107:155704.
13. Strandburg KJ (1988) Two-dimensional melting. *Rev Mod Phys* 60:161–207.
14. Zahn K, Maret G (2000) Dynamic criteria for melting in two dimensions. *Phys Rev Lett* 85:3656–3659.
15. Gasser U, Eisenmann C, Maret G, Keim P (2010) Melting of crystals in two dimensions. *Chemphyschem* 11:963–970.
16. Kegel WK, van Blaaderen A (2000) Direct observation of dynamical heterogeneities in colloidal hard-sphere suspensions. *Science* 287:290–293.
17. Weeks ER, Crocker JC, Levitt AC, Schofield A, Weitz DA (2000) Three-dimensional direct imaging of structural relaxation near the colloidal glass transition. *Science* 287:627–631.
18. Ebert F, Dillmann P, Maret G, Keim P (2009) The experimental realization of a two-dimensional colloidal model system. *Rev Sci Instrum* 80:083902.
19. Pusey PN, van Megen W (1986) Phase behaviour of concentrated suspensions of nearly hard colloidal spheres. *Nature* 320:340–342.
20. Narumi T, Franklin SV, Desmond KW, Tokuyama M, Weeks ER (2011) Spatial and temporal dynamical heterogeneities approaching the binary colloidal glass transition. *Soft Matter* 7:1472–1482.
21. Peierls R (1934) Bemerkungen über umwandlungstemperaturen. *Helv Phys Acta* 7: 81–83.
22. Landau LD (1937) Zur theorie der phasenumwandlungen II. *Phys Z Sowjetunion* 11:26–35.
23. Mermin ND, Wagner H (1966) Absence of ferromagnetism or antiferromagnetism in one- or two-dimensional isotropic Heisenberg models. *Phys Rev Lett* 17:1133–1136.
24. Mermin ND (1968) Crystalline order in two dimensions. *Phys Rev* 176:250–254.
25. Illing B, et al. (2017) Mermin-Wagner fluctuations in 2D amorphous solids. *Proc Natl Acad Sci USA* 114:1856–1861.
26. Klix CL, Maret G, Keim P (2015) Discontinuous shear modulus determines the glass transition temperature. *Phys Rev X* 5:041033.
27. Mazoyer S, Ebert F, Maret G, Keim P (2009) Dynamics of particles and cages in an experimental 2D glass former. *Europhys Lett* 88:66004.
28. Gray AT, Mould E, Royall CP, Williams I (2015) Structural characterisation of polycrystalline colloidal monolayers in the presence of aspherical impurities. *J Phys Condens Matter* 27:194108.
29. Donev A, Stillinger FH, Torquato S (2006) Do binary hard disks exhibit an ideal glass transition? *Phys Rev Lett* 96:225502.
30. Kelleher CP, et al. (2015) Charged hydrophobic colloids at an oil-aqueous phase interface. *Phys Rev E* 92:062306.
31. Steinhardt PJ, Nelson DR, Ronchetti M (1983) Bond-orientational order in liquids and glasses. *Phys Rev B* 28:784–805.
32. Weeks ER, Crocker JC, Weitz DA (2007) Short- and long-range correlated motion observed in colloidal glasses and liquids. *J Phys Condens Matter* 19:205131.
33. Shiba H, Yamada Y, Kawasaki T, Kim K (2016) Unveiling dimensionality dependence of glassy dynamics: 2D infinite fluctuation eclipses inherent structural relaxation. *Phys Rev Lett* 117:245701.
34. Rabani E, Gezelter JD, Berne BJ (1997) Calculating the hopping rate for self-diffusion on rough potential energy surfaces: Cage correlations. *J Chem Phys* 107: 6867–6876.
35. Weeks ER, Weitz DA (2002) Properties of cage rearrangements observed near the colloidal glass transition. *Phys Rev Lett* 89:095704.
36. Yunker P, Zhang Z, Aptowicz KB, Yodh AG (2009) Irreversible rearrangements, correlated domains, and local structure in aging glasses. *Phys Rev Lett* 103:115701.
37. Zhang Z, Yunker PJ, Habdas P, Yodh AG (2011) Cooperative rearrangement regions and dynamical heterogeneities in colloidal glasses with attractive versus repulsive interactions. *Phys Rev Lett* 107:208303.
38. Fröhlich J, Pfister C (1981) On the absence of spontaneous symmetry breaking and of crystalline ordering in two-dimensional systems. *Commun Math Phys* 81:277–298.
39. Kapfer SC, Krauth W (2015) Two-dimensional melting: From liquid-hexatic coexistence to continuous transitions. *Phys Rev Lett* 114:035702.
40. Shiba H, Kawasaki T, Onuki A (2012) Relationship between bond-breakage correlations and four-point correlations in heterogeneous glassy dynamics: Configuration changes and vibration modes. *Phys Rev E* 86:041504.
41. Thorneywork AL, Roth R, Aarts DG, Dullens RP (2014) Communication: Radial distribution functions in a two-dimensional binary colloidal hard sphere system. *J Chem Phys* 140(16):161106.
42. Crocker JC, Grier DG (1996) Methods of digital video microscopy for colloidal studies. *J Colloid Interface Sci* 179:298–310.